

BCSJ Award Article

Dendrimer Effects on Intermolecular Energy-Transfer of Photoexcited Triplet States of Dendritic Multiporphyrin Arrays and Electron Transfer vs Fullerene[60]

Hongxia Luo,[†] Myung-Seok Choi,[1,2,††] Yasuyuki Araki, Osamu Ito,* and Takuzo Aida*[,1,2]

Institute of Multidisciplinary Research for Advanced Materials, Tohoku University, CREST (JST), Katahira 2-1-1, Aoba-ku, Sendai 980-8577

[1]ERATO Nanospace Project, Japan Science and Technology Corporation (JST), 2-41 Aomi, Koto-Ku, Tokyo 115-0064

[2]Department of Chemistry and Biotechnology, Graduate School of Engineering, The University of Tokyo, 7-3-1 Hongo, Bunkyo-ku, Tokyo 113-8656

Received August 17, 2004; E-mail: ito@tagen.tohoku.ac.jp

Photochemical and photophysical properties of the triplet excited states of dendritic multiporphyrins arrays (nP_{Zn}, n = 1, 3, and 7) have been investigated by measuring the nanosecond transient absorption spectra in the visible and near-IR regions with changing the generation number. Intermolecular triplet–triplet annihilation rates decrease with the dendrimer generation, which was interpreted on a proposed kinetic model assuming that the excited triplet energy almost localizes in one P_{Zn} unit in nP_{Zn}. In the presence of C_{60}, intermolecular electron-transfer takes place via the excited triplet states of nP_{Zn} ($^3nP_{Zn}$*), yielding the cation radical of nP_{Zn} ($nP_{Zn}^{\bullet+}$) and the anion radical of C_{60} ($C_{60}^{\bullet-}$) in PhCN. Deceleration of the electron-transfer rate-constants from $1P_{Zn}$ to $3P_{Zn}$ and the acceleration from $3P_{Zn}$ to $7P_{Zn}$ were observed, in which the latter tendency was interpreted by considering an increase in effective encounter radius for $^37P_{Zn}$*. The observed small change of the rate constants for back electron transfer between the oppositely charged species with the dendrimer generation was also reasonably interpreted by taking a smaller effective radius due to electrostatic attraction into consideration. Dendrimer generation effect was also observed for the intermolecular hole-transfer process.

Since the first reported preparation of porphyrin dendrimers in 1993,[1] a number of functionalized porphyrin dendrimers have been synthesized and characterized.[2–26] Due to their unique morphologies, photophysical and photochemical properties of the porphyrin dendrimers have been explored.[5,12,13,17,19] There are two types of dendrimers relating to photochemical interests. (1) Chromophore is at the core and (2) each dendrimer has chromophores all over the molecules. Aida et al. reported light-harvesting dendritic porphyrinatozinc arrays to allow efficient channel of visible photons.[8,18] In recent years, the photophysics and photochemistry of fullerene–porphyrin mixed systems in polar solvents have attracted a great attention.[27–30] Kimura et al. reported that fullerenes formed inclusion complexes with a dendrimer having a porphyrin in a core.[31] For fullerene dendrimers linked with tetraphenyl porphyrin chromophores,[32] photoinduced electron transfer has been investigated. Dendritic multiporphyrin arrays covalently bonded with C_{60} have also been synthesized and their intramolecular charge-separation and charge-recombination properties have been investigated.[33–35]

In the present study, we report the photochemical and photophysical properties of the excited triplet state of the dendritic multiporphyrin arrays with fanwise shapes (nP_{Zn}, n = 1, 3, and 7 in Fig. 1), in which most of the porphyrin moieties are exposed. This permits us to study the intermolecular reactions such as photoinduced energy- and electron-transfer processes of the excited states of nP_{Zn}. The rate constants of these processes for the excited triplet state of nP_{Zn} ($^3nP_{Zn}$*) have been determined by the laser flash photolysis that observes the transient absorption spectra in the visible/near-IR regions. For electron transfer, C_{60} was employed as an electron acceptor, since the absorption band of the radical anion of C_{60} ($C_{60}^{\bullet-}$) does not overlap with the transient absorption of $^3nP_{Zn}$*, which permitted us to evaluate the precise rate constants to reveal the dendrimer generation effects. Furthermore, hole-shifting processes have been investigated to obtain useful information applicable to optoelectronic devices. In order to interpret these data, we proposed some kinetic models that include the radii of nP_{Zn} and probability of collision with the target excited moiety in the dendric multiporphyrin arrays.

† Present address: Department of Chemistry, Renmin University of China, Beijing, 100872, China

†† Present address: SONY Corporation, Fusion Domain Laboratory, Tokyo 144-0033

Published on the web March 11, 2005; DOI 10.1246/bcsj.78.405

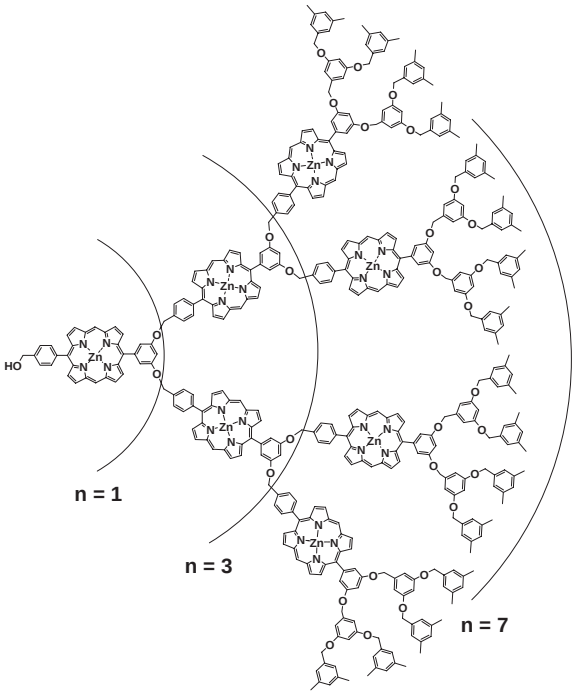

Fig. 1. Structures of dendritic multiporphyrin arrays (nP_{Zn}).

Experimental

Materials. Dendric multiporphyrin arrays (nP_{Zn}) were synthesized using the method described in the previous papers.[18] C_{60} (purity of 99.9%) was obtained from Texas Fullerenes Corporation. The aromatic amine (ArA; 4,5-dihydro-5-[4-(diethylamino)-phenyl]-3-{2-[4-(diethylamino)phenyl]ethenyl}-1-phenylpyrazole) was available from Anan Koryo LTD, Japan. Solvents were of spectroscopic grade and HPLC grade.

Measurements. Steady-state absorption spectra in the visible and near-IR regions were measured on a Jasco V570 DS spectrophotometer. Nanosecond transient absorption spectra in the visible and near-IR regions were observed by the laser-flash photolysis apparatus using the SHG (532 nm) light of a Nd:YAG laser (Quanta-Ray; 6 ns fwhm) as an excitation source. For time-scale measurements shorter than 10 ns, a Si-PIN photodiode module (400–600 nm) and a Ge-APD module (600–1600 nm) were employed as detectors for monitoring the light from a pulsed Xe-lamp. For time-scale measurements longer than 10 ns, an InGaAs-PIN photodiode was used as a detector for monitoring light from a continuous Xe-lamp (150 W). The sample solutions were deaerated by bubbling with argon gas before measurements. The laser photolysis was performed for each solution in a rectangular quartz cell with a 10 mm optical path. All the measurements were carried out at 23 °C. Details of the experimental procedures are described elsewhere.[27–30] Cyclic voltammograms were measured using a conventional three-electrode system on a BAS CV-50W potentiostat/galvanostat. A platinum disk electrode (1 mm in diameter) was used as a working electrode. A platinum wire served as a counter electrode. An Ag/AgCl electrode was used as the reference electrode. The potentials were referenced to an internal ferrocene/ferrocenium (Fc/Fc^+) redox couple. Molecular structures were optimized by the MM3 force field modified in MacroModel package.

Results and Discussion

Optimized Structures. Figure 2 shows an optimized structure of $7P_{Zn}$ calculated by the MM3 force field modified in MacroModel package. It is clear that $7P_{Zn}$ is a flat molecule. For $3P_{Zn}$ and $1P_{Zn}$, optimized structures are similar to those of the compartments. The maximal radii of nP_{Zn} including poly(benzyl ether) dendron substituents are evaluated to be 14, 29, and 71 Å for $1P_{Zn}$, $3P_{Zn}$, and $7P_{Zn}$, respectively.

Cyclic Voltammograms. Each cyclic voltammogram showed a reversible cycle in the scan range of −0.2 to 0.8 V vs Fc/Fc^+. The first oxidation potentials were observed to be 0.33, 0.31, and 0.29 V vs Fc/Fc^+ for $1P_{Zn}$, $3P_{Zn}$, and $7P_{Zn}$, respectively. Slight decrease of the oxidation potentials with dendrimer generation suggests a weak interaction among

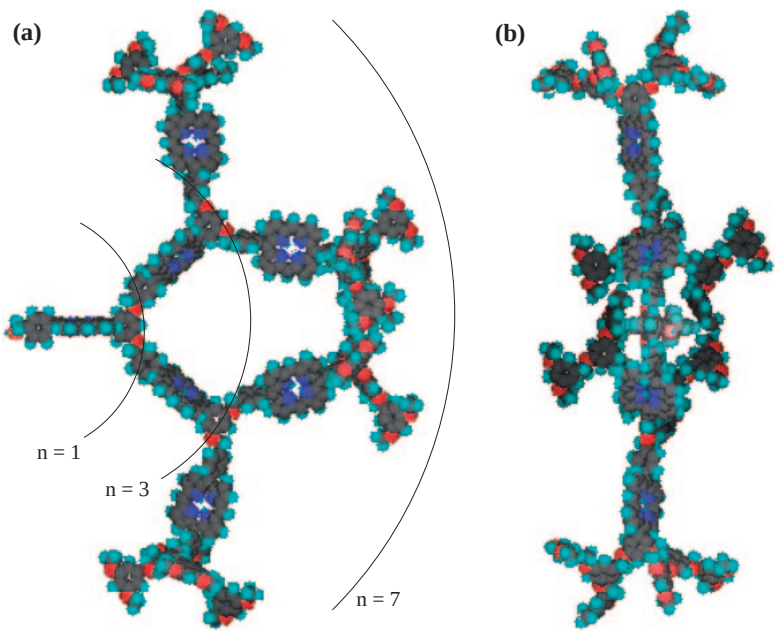

Fig. 2. (a) Facade view and (b) side view of dendritic multiporphyrin arrays (nP_{Zn}) structure optimized by MM3 force field calculation.

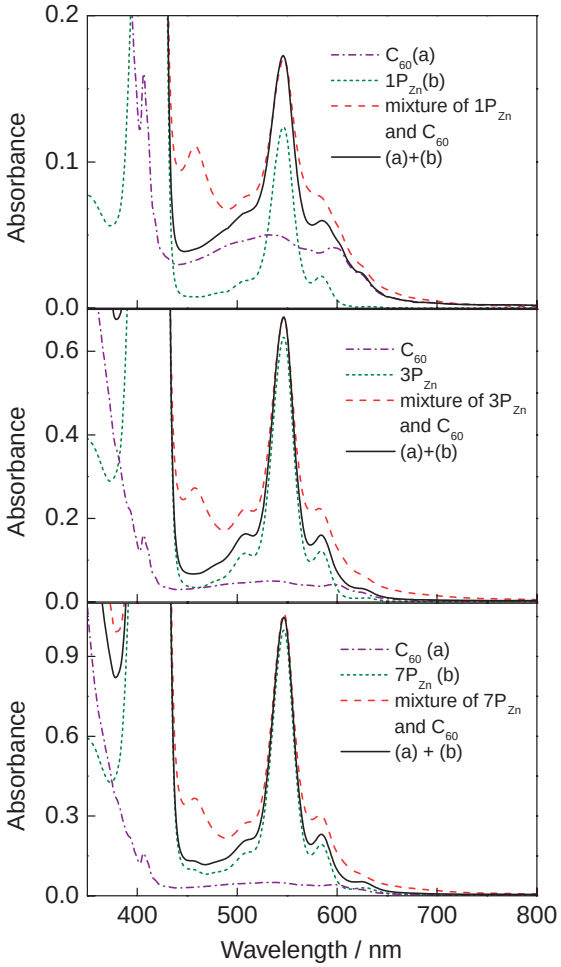

Fig. 3. Steady-state absorption spectra of (a) C_{60} (0.1 mmol dm^{-3}), (b) nP_{Zn} (0.02 mmol dm^{-3}), and mixture of nP_{Zn} (0.02 mmol dm^{-3}) and C_{60} (0.1 mmol dm^{-3}), and calculated (a) + (b) in PhCN.

the P_{Zn} moieties in the dendrimers.

Steady-State Absorption Spectra. Figure 3 shows absorption spectra of nP_{Zn} (n = 1, 3, and 7) in PhCN, where the absorption peaks at 550 nm with wings at 500 and 580 nm are attributed to the Q bands of the porphyrin chromophores. The absorption intensities were almost proportional to the number of P_{Zn} moieties in the dendrimers. In each spectrum, the absorption spectrum of C_{60} is shown for comparison. The absorption intensities in the visible region of each absorption spectrum of the mixture of nP_{Zn} (n = 1, 3, and 7) with C_{60} are slightly larger than the corresponding added spectrum of the two components, suggesting an appreciable interaction between nP_{Zn} and C_{60}. Especially, a new weak peak was observed at 433 nm.

Nanosecond Transient Absorption Spectra. Excited Triplet State: Transient absorption spectra of $3P_{Zn}$ in anisole are shown in Fig. 4. Anisole was employed as a solvent for dissolving $3P_{Zn}$ well with less polarity, preventing extra processes such as photo-electron ejection. Immediately after the 6 ns laser pulse excitation, the main absorption peaks appeared at 460 nm with a weak band at 840 nm; these were attributed to the triplet–triplet transition.[36–39] These absorption intensities of

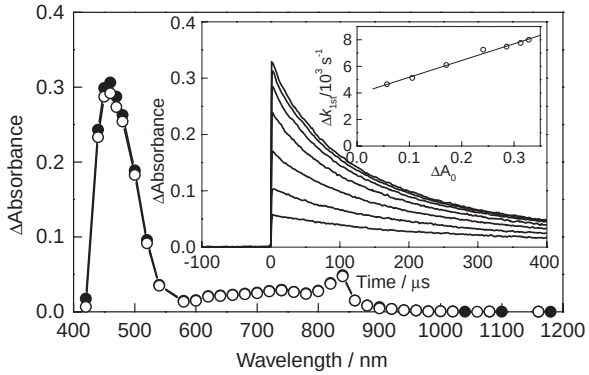

Fig. 4. Nanosecond transient spectra observed by the 560 nm laser light excitation of $3P_{Zn}$ (0.02 mmol dm^{-3}) in anisole at 0.25 μs (–●–) and 2.5 μs (–○–). Inset: Laser power dependence of the decay time-profile and plots of Eq. 3 at 460 nm.

^{3}3P$_{Zn}$* decayed within 400–500 μs, depending on the laser power (inset in Fig. 4). The decay profiles showed mixed first- and second-order kinetics, which indicates that following two processes (Eq. 1 and Eq. 2) take place simultaneously.[40] When we employed the maximal absorbance (ΔA_0) of ^{3}3P$_{Zn}$* of 0.33 and its molar extinction coefficient (ε_T) of 9.0×10^4 mol^{-1} dm^3 cm^{-1} at 460 nm,[39] the maximal concentration of ^{3}3P$_{Zn}$* generated by one pulsed laser light shot was estimated to be 0.004 mmol dm^{-3}, indicating that ca. 20% of $3P_{Zn}$ was photo-excited. Thus, the probability that more than two P_{Zn} units are excited by one laser light exposure is very low. For $7P_{Zn}$, similar transient spectra and decay time profiles were observed. Therefore, intermolecular T–T annihilation (Eq. 2) can be considered as a decay process of $^3nP_{Zn}$* in addition to the intrinsic deactivation of $^3nP_{Zn}$* (Eq. 1):

$$^3nP_{Zn}^* \xrightarrow{k_0^T(=1/\tau_0^T)} nP_{Zn} \quad (1)$$

$$^3nP_{Zn}^* + {}^3nP_{Zn}^* \xrightarrow{k_{T-T}} {}^1nP_{Zn}^* + nP_{Zn} \text{ etc.} \quad (2)$$

The first- and second-order rate constants can be separated by the following Eq. 3:[40]

$$-\mathrm{d}[\Delta A_{init}]/\mathrm{d}t = \Delta k_{1st}{}^T = k_0{}^T + (2k_{T-T}/\varepsilon_T)\Delta A_0 \quad (3)$$

where $k_{1st}{}^T$ refers to the apparent first-order rate constant evaluated from the slope of the initial part (ΔA_{init}) in the first-order plot; $k_0{}^T$ refers to the intrinsic rate constant for the decay of $^3nP_{Zn}$* (Eq. 1), which can be evaluated from the intercept of the plots of Eq. 3 as shown in the inset of Fig. 4. The inversed values of $k_0{}^T$ correspond to $\tau_0{}^T$ values, which are in the range of 240–260 μs (Table 1). With an increase in the dendrimer

Table 1. Intrinsic Decay Rate Constants ($k^0{}_T$), Lifetimes ($\tau^0{}_T$), and T–T Annihilation Rate Constants ($k_{T-T}{}^{obs}$) of $^3nP_{Zn}$*'s in Anisole

nP_{Zn}	$k^0{}_T/s^{-1}$	$\tau^0{}_T/\mu s$	$k_{T-T}{}^{obs}/mol^{-1}\,dm^3\,s^{-1}$ a)
$1P_{Zn}$	$(4.1 \pm 0.2) \times 10^3$	250 ± 10	$(2.3 \pm 0.1) \times 10^9$
$3P_{Zn}$	$(3.9 \pm 0.2) \times 10^3$	260 ± 10	$(1.2 \pm 0.1) \times 10^9$
$7P_{Zn}$	$(3.9 \pm 0.2) \times 10^3$	260 ± 10	$(1.2 \pm 0.1) \times 10^9$

a) $\varepsilon_{460\ nm} = 9.0 \times 10^4$ mol^{-1} dm^3 cm^{-1} for ^{3}ZnTPP* was employed.[36]

generation, a slight increase of $\tau_0{}^T$ values was found, indicating that the relaxation process from $^3nP_{Zn}$* to the ground state is slightly slowed down. The slopes of the plots of $\Delta k_{1st}{}^T$ vs ΔA_0 (initial absorbance) give the ratio of $2k_{T-T}/\varepsilon_T$, where k_{T-T} denotes the rate constant for T–T annihilation (Eq. 2). On employing $\varepsilon_T = 9.0 \times 10^4$ mol^{-1} dm^3 cm^{-1} at 460 nm,[39] the $k_{T-T}{}^{obs}$ values are evaluated to be $(1.2–2.3) \times 10^9$ mol^{-1} dm^3 s^{-1} (Table 1), which are about a half of the diffusion-controlled limit ($k_{diff} = 6 \times 10^9$ mol^{-1} dm^3 s^{-1} in anisole).[41] The $k_{T-T}{}^{obs}$ values tend to decrease with an increase in the generation number from $1P_{Zn}$ to $3P_{Zn}$ and $7P_{Zn}$ by a factor of ca. 1/2.

As the first approximation that the excited triplet state delocalizes in the whole of nP_{Zn} molecules, the rate constants for encounter between two $^3nP_{Zn}$*'s ($k_{T-T}{}^{pred1}$) can be thought to be proportional to the frequency factor (Z), as represented by Eq. 4:[42]

$$k_{T-T}{}^{pred1} \propto Z \propto \sigma_{T-T}\mu_{T-T}{}^{-1/2} \quad (4)$$

where σ_{T-T} refers to the cross-section which is proportional to the square of the radius of $^3nP_{Zn}$*; μ_{T-T} refers to the reduced mass. Thus, the ratio of the $k_{T-T}{}^{pred1}$ values for $1P_{Zn}$:$3P_{Zn}$:$7P_{Zn}$ was evaluated to be 1:1.25:1.92. This ratio has the opposite tendency to the $k_{T-T}{}^{obs}$ values. This discrepancy between the $k_{T-T}{}^{obs}$ values and the $k_{T-T}{}^{pred1}$ values may be attributed to the localization of the excited triplet energy on a P_{Zn} unit in nP_{Zn}. Thus, the probability (P_{T-T}) for energy transfer to encounter the $^3P_{Zn}$* moiety in nP_{Zn} should be introduced as in Eq. 5:

$$k_{T-T}{}^{pred2} \propto ZP_{T-T} \quad (5)$$

where the ratio of P_{T-T} is assumed to be inversely proportional to the number of P_{Zn} in nP_{Zn}; that is, 1:1/3:1/7 for ^{3}1P_{Zn}*:^{3}3P_{Zn}*:^{3}7P_{Zn}. Comparison of the $k_{T-T}{}^{obs}$ values with the ratio of $k_{T-T}{}^{pred2}$ shows a similar tendency, as shown in Fig. 5. Slight deviation suggests that the localization of the $^3P_{Zn}$* state is not strictly limited in one unit, but the $^3P_{Zn}$* state slightly expands to the neighboring P_{Zn} moieties, resulting in an increase of the effective radii of the $^3P_{Zn}$* state with an increase of the dendrimer generation.

Photoinduced ET from $^3nP_{Zn}$* to C_{60}: Upon excitation of the $3P_{Zn}$ moiety at 560 nm in PhCN with the presence of C_{60}, transient absorption spectra were observed as shown in

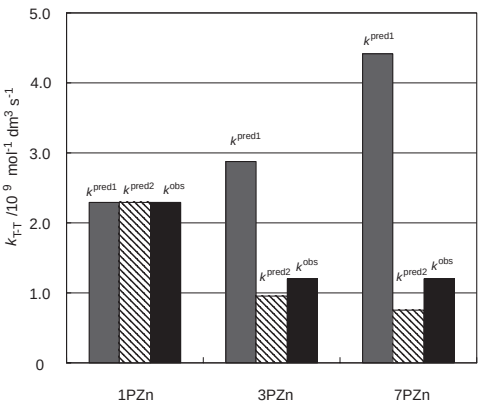

Fig. 5. Comparison of $k_{T-T}{}^{obs}$ with $k_{T-T}{}^{pred1}$ and $k_{T-T}{}^{pred2}$.

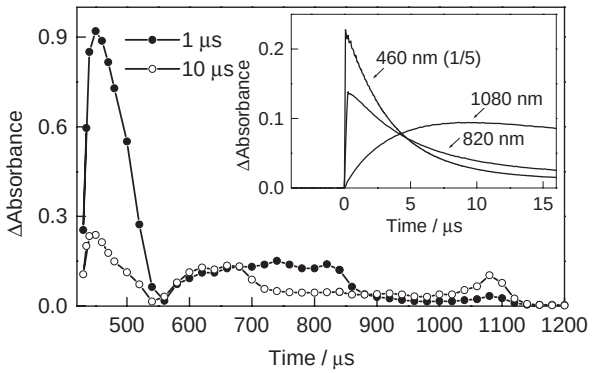

Fig. 6. Nanosecond transient absorption spectra of $3P_{Zn}$ (0.05 mmol dm^{-3}) in the presence of C_{60} (0.10 mmol dm^{-3}) in deaerated PhCN after the 560 nm laser irradiation. Inset: Time profiles of absorbance at 460, 820, and 1080 nm.

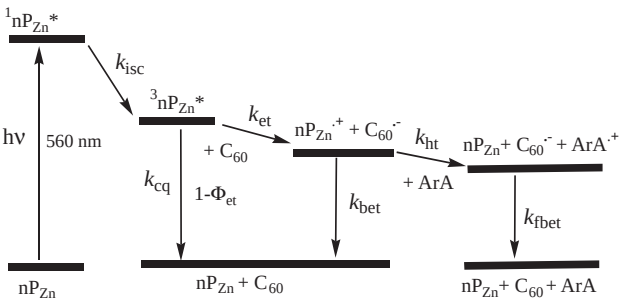

Fig. 7. Energy diagram for processes occurring from excitation of nP_{Zn} in the presence of C_{60} and ArA in PhCN.

Fig. 6. Under the concentration of $3P_{Zn}$ (0.05 mmol dm^{-3}), 96% of the 560-nm light was absorbed by $3P_{Zn}$ in the presence of C_{60} (0.1 mmol dm^{-3}). At 1-μs delayed time after the laser light excitation, the transient absorption bands due to ^{3}3P_{Zn}* appeared at 460 and 820 nm, while at 10-μs delayed time, the absorption bands due to $C_{60}{}^{\bullet-}$ at 1080 nm rose together with concomitant decays of the absorption bands due to ^{3}3P_{Zn}*.[43,44] The absorption bands at 440 and 600–700 nm are observed in the spectrum at 10 μs, which are attributed to the radical cation of $3P_{Zn}$ ($3P_{Zn}{}^{\bullet+}$).[27] This observation clearly indicates that electron transfer takes place from ^{3}3P_{Zn}* to C_{60}, producing $C_{60}{}^{\bullet-}$ and $3P_{Zn}{}^{\bullet+}$. Similar transient absorption spectra were observed for $1P_{Zn}$ and $7P_{Zn}$ in the presence of C_{60}. In the case of 0.05 mmol dm^{-3} of $1P_{Zn}$ and $7P_{Zn}$, 87% and 99% of $1P_{Zn}$ and $7P_{Zn}$ were excited in the presence of C_{60} (0.1 mmol dm^{-3}), respectively. The energy diagram of these processes is schematically represented in Fig. 7. Exothermic electron transfer process was confirmed from the negative free-energy changes for electron transfer ($\Delta G_{et}{}^o$) from $^3nP_{Zn}$*'s to C_{60} in PhCN, as calculated by the Rehm–Weller equation (Table 2).[45]

The electron transfer rate constants (k_{et}) were evaluated from the quenching rate constants (k_q) of $^3nP_{Zn}$*'s in the presence of C_{60}. Decays of $^3nP_{Zn}$*'s obey first-order kinetics, giving the first-order rate constant ($k_{1st\text{-}order}$), which increases with the C_{60} concentrations. Such a pseudo-first order relation indicates that the intermolecular dynamic events are predominant-

Table 2. Quenching Rate-Constants (k_q) of ^3nP_Z* by C_{60}, Quantum Yields (Φ_{et}) and Electron-Transfer Rate-Constants (k_{et}^{obs}) from $^3nP_{Zn}$* to C_{60}, and Back Electron-Transfer Rate-Constants (k_{bet}^{2nd}) from $C_{60}^{\bullet-}$ to $nP_{Zn}^{\bullet+}$ in PhCN

	E_{ox} a) /V	ΔG_{et}^0 b) /eV	$k_q \times 10^{-9}$ /mol^{-1} dm^3 s^{-1}	Φ_{et} c)	$k_{et}^{obs} \times 10^{-9}$ /mol^{-1} dm^3 s^{-1}	k_{bet}^{2nd} c) $\times 10^{-9}$ /mol^{-1} dm^3 s^{-1}
$1P_{Zn}$	0.33	−0.26	1.6 ± 0.1	0.63 ± 0.03	1.0 ± 0.1	5.5 ± 0.3
$3P_{Zn}$	0.31	−0.28	1.4 ± 0.1	0.36 ± 0.02	0.5 ± 0.1	6.0 ± 0.3
$7P_{Zn}$	0.29	−0.31	2.1 ± 0.1	0.56 ± 0.03	1.2 ± 0.1	5.2 ± 0.3

a) vs Fc/Fc^+. b) The values of ΔG_{et}^0 were evaluated from the Rehm–Weller equation,[45] employing the values of E_{red} and E_T for C_{60} to be −0.93 V and 1.54 eV, respectively.[42–44] c) $\varepsilon_{RA} = 12100$ mol^{-1} dm^3 cm^{-1} for $C_{60}^{\bullet-}$.[37,39]

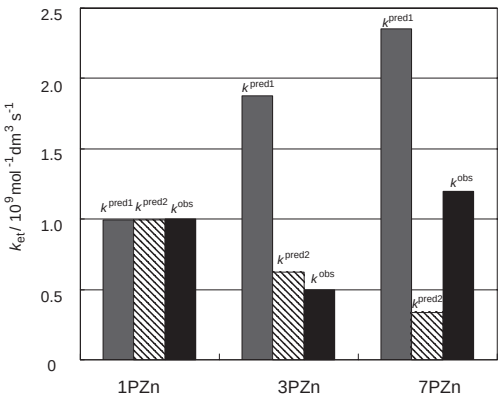

Fig. 8. Comparison of k_{et}^{obs} with k_{et}^{pred1} and k_{et}^{pred2}.

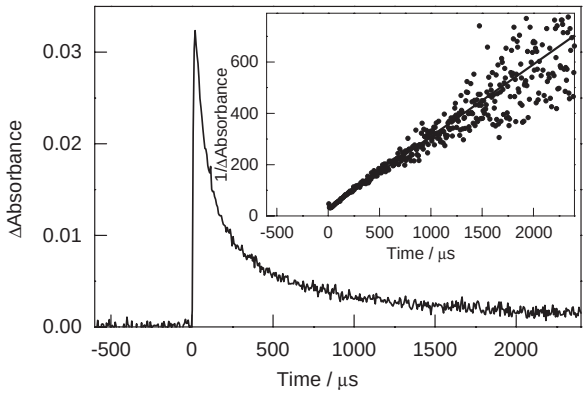

Fig. 9. Decays of $C_{60}^{\bullet-}$ at 1080 nm in the mixture of $3P_{Zn}$ (0.05 mmol dm^{-3}) + C_{60} (0.1 mmol dm^{-3}) in PhCN after the 560 nm laser irradiation. Inset: Second-order plot.

ly occurring, even though a part of nP_{Zn} and C_{60} is interacting in the ground state as presumed from the absorption spectra in Fig. 3.[46] The pseudo-first-order plots give a straight line; the slope gives k_q of $^3nP_{Zn}$* by C_{60} as summarized in Table 2. From the rise of $C_{60}^{\bullet-}$, similar k_q values in the range of (1.4–2.1) $\times 10^9$ mol^{-1} dm^3 s^{-1} were obtained. A smaller k_q value was found for ^{3}3P_{Zn}*, which indicates that the two P_{Zn} units in the ground state sterically hinder an approach of C_{60} to $^3P_{Zn}$*, when the $^3P_{Zn}$* state is almost localized in one P_{Zn} unit in $3P_{Zn}$. On the other hand, a larger k_q value was found for ^{3}7P_{Zn}*, which suggests that the huge dendrimer P_{Zn} moieties in ^{3}7P_{Zn}* wrap C_{60}.[31]

The quantum yield (Φ_{et}) of electron transfer from $^3nP_{Zn}$* to C_{60} was estimated from the ratio of the maximal concentration of $C_{60}^{\bullet-}$ ($[C_{60}^{\bullet-}]_{max}$) to the initial concentration of $^3nP_{Zn}$* ($[^3nP_{Zn}^*]_{init}$), employing the reported molar extinction coefficient of $C_{60}^{\bullet-}$ ($\varepsilon_{RA} = 12100$ mol^{-1} dm^3 cm^{-1}).[43,44] On plotting $[C_{60}^{\bullet-}]_{max}/[^3nP_{Zn}^*]_{init}$ with $[C_{60}]$, the ratio showed saturation at higher $[C_{60}]$; the saturation ratios can be put equal to the Φ_{et} values,[47,48] which are listed in Table 2. The Φ_{et} values are in the range of 0.36–0.63; the minimum value was observed for ^{3}3P_{Zn}*, suggesting that the P_{Zn} moieties in ^{3}3P_{Zn}* hinder the approach of C_{60} to the $^3P_{Zn}$* moiety. The Φ_{et} value for ^{3}7P_{Zn}* is rather similar to that of ^{3}1P_{Zn}*. This result suggests that stronger interactions are likely to operate between C_{60} and $7P_{Zn}$. The k_{et}^{obs} values were evaluated from the relationship: $k_{et}^{obs} = k_q \times \Phi_{et}$.[47,48] The k_{et}^{obs} values are in the range of (0.5–1.2) $\times 10^9$ mol^{-1} dm^3 s^{-1}; ^{3}3P_{Zn}* shows a minimum value, while ^{3}7P_{Zn}* shows a maximal value. It is notable that the efficient electron-transfer ability of ^{3}7P_{Zn}* found in the present study may be related to the flat molecular surface with a large pocket capable of trapping C_{60}.

In general, the bimolecular electron-transfer rate-constant (k_{et}) between $^3nP_{Zn}$* and C_{60} can be represented as Eq. 6:[49]

$$(k_{et}^{-1}) = k_{diff}^{-1} + Z^{-1} \exp[(\lambda/4)(1 + \Delta G^0/\lambda)2/k_B T] \quad (6)$$

where reorganization (λ) was assumed to be 0.8 eV for electron transfer from $^3nP_{Zn}$* to C_{60} on the basis of the reported values.[49] Then, on putting $k_{diff} = 5.3 \times 10^9$ mol^{-1} dm^3 s^{-1} in PhCN at $T = 300$ K,[41] the k_{et} values were calculated, which refer to k_{et}^{pred1}. As shown in Fig. 8, the k_{et}^{pred1} values increase with the dendrimer generation; however, this trend is not consistent with that of the k_{et}^{obs} values. On introducing a probability factor for electron transfer ($P_{et} = 1{:}1/3{:}1/7$ for $1P_{Zn}{:}3P_{Zn}{:}7P_{Zn}$), the values of k_{et}^{pred2} ($= k_{et}^{pred1} \times P_{et}$) were evaluated as shown in Fig. 8. A decreasing tendency of the k_{et}^{obs} values from $1P_{Zn}$ to $3P_{Zn}$ is in agreement with that of k_{et}^{pred2}. However, an increasing tendency of the k_{et}^{obs} value from $1P_{Zn}$ (and $3P_{Zn}$) to $7P_{Zn}$ is not predicted even in the k_{et}^{pred2} value; as a reason for this, the increases of the effective radius of the $^3P_{Zn}$* state in $7P_{Zn}$ and of the trapping ability of $7P_{Zn}$ can be considered.

Back Electron-Transfer: After reaching maximum concentration by electron-transfer, $C_{60}^{\bullet-}$ begins decaying, as shown in long time-scale measurements (Fig. 9). Linear relationships of the second-order plots (inset in Fig. 9) indicate that the radical ions are separately solvated as free ions. From the second-order plots, the rate constants for back electron transfer (k_{bet}^{2nd}) were evaluated as ratios to ε_{RA}. On employing the reported ε_{RA} value,[43,44] the k_{bet}^{2nd} values are evaluated

in the range of $(5.2–6.0) \times 10^9$ $mol^{-1}\,dm^3\,s^{-1}$ as listed in Table 2. The $k_{bet}{}^{2nd}$ values are almost the same within the experimental error and are close to k_{diff} in PhCN.[41] The diffusion-controlled reactions may be mainly controlled by Eq. 4, predicting a smooth increase of the $k_{bet}{}^{2nd}$ values with the dendrimer generation; however, when the positive charge is mainly localized on a P_{Zn} unit, a ratio of the probability for the encounter of $C_{60}{}^{\bullet-}$ and $P_{Zn}{}^{\bullet+}$ (P_{bet}) must be introduced again. For example, on assuming that the ratios for P_{bet} are about a half of those of P_{et} ($P_{bet} = 1{:}2/3{:}2/7$ for $1P_{Zn}{}^{\bullet+}{:}3P_{Zn}{}^{\bullet+}{:}7P_{Zn}{}^{\bullet+}$), the invariant tendency of the observed $k_{bet}{}^{2nd}$ values with the dendrimer generation can be well reproduced. As one of reasons for high P_{bet}, one can consider that $C_{60}{}^{\bullet-}$ hits the $P_{Zn}{}^{\bullet+}$ moiety in $nP_{Zn}{}^{\bullet+}$ in higher probability in the encounter between the oppositely charged species. As other reasons, one can also consider a slight delocalization of the hole of $P_{Zn}{}^{\bullet+}$ to the neighboring P_{Zn} moieties.

Hole-Shifting from $nP_{Zn}{}^{\bullet+}$ to Aromatic Amines: On addition of aromatic amine (ArA; Fig. 10) to the mixture of $7P_{Zn}$ and C_{60} in PhCN, transient absorption spectra were observed, as shown in Fig. 11, upon excitation at 560 nm. The absorption bands of $^37P_{Zn}{}^*$ appearing at 460 and 820 nm immediately after the laser light excitation decayed with producing $C_{60}{}^{\bullet-}$ at 1080 nm, as shown in the inserted time profile of Fig. 11; the absorption band of $7P_{Zn}{}^{\bullet+}$ was also anticipated to appear at 620 nm, although in this region other strong absorption bands overlapped. In the spectrum at 10 μs, new absorption bands were observed at 620 and 1300 nm, which were attributed to the radical cation of ArA ($ArA^{\bullet+}$).[50] Thus, it is confirmed that the radical cation (hole) of $7P_{Zn}{}^{\bullet+}$ shifts to ArA, producing $ArA^{\bullet+}$ as drawn in Fig. 10. This hole shift is possible, because the oxidation potential of ArA (−0.02 V vs Fc/Fc^+) is much lower than those of nP_{Zn} (0.4–0.5 V vs Fc/Fc^+).[50] From the rise of $ArA^{\bullet+}$, the rate constants for hole-shifting process (k_{hs}) were evaluated to be $(3.1–5.8) \times 10^7$ $mol^{-1}\,dm^3\,s^{-1}$ for nP_{Zn}; a smooth increase of the k_{hs} values with the dendrimer generation was observed, which is a rather similar tendency to that of $k_{et}{}^{pred1}$. For the hole-shift process

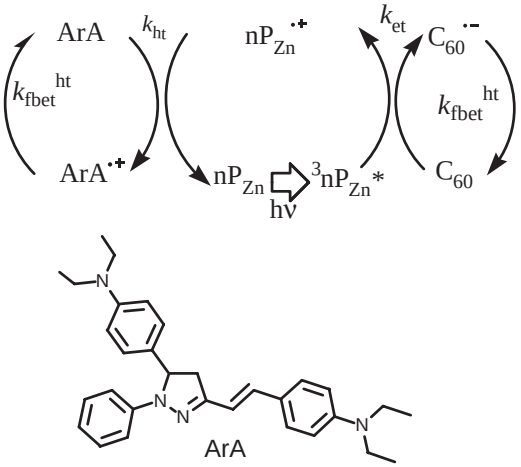

4,5-dihydro-5-[4-(diethylamino)phenyl]-3-{2-[4-(diethylamino)phenyl]ethenyl}-1-phenylpyrazole

Fig. 10. Hole-shift system and structure of ArA.

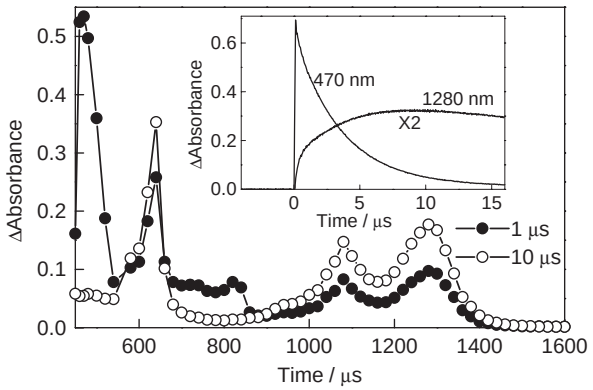

Fig. 11. Nanosecond transient absorption spectra obtained by 560 nm laser excitation of $7P_{Zn}$ (0.05 mmol dm^{-3}) in the presence of C_{60} (0.10 mmol dm^{-3}) and ArA (0.6 mmol dm^{-3}) in deaerated PhCN at 1 μs (–●–) and 10 μs (–○–). Inset: Time profiles of absorbance at 470 and 1280 nm.

Table 3. Hole-Shifting Rate Constants (k_{hs}) and Final Back Electron-Transfer Rate-Constants after Hole-Shifting ($k_{fbet}{}^{hs}$) in PhCN

	k_{hs}/$mol^{-1}\,dm^3\,s^{-1}$	$k_{fbet}{}^{hs}$[a]/$mol^{-1}\,dm^3\,s^{-1}$
$1P_{Zn}$	$(3.1 \pm 0.2) \times 10^7$	$(2.7 \pm 0.2) \times 10^8$
$3P_{Zn}$	$(4.2 \pm 0.2) \times 10^7$	$(2.8 \pm 0.2) \times 10^8$
$7P_{Zn}$	$(5.8 \pm 0.3) \times 10^7$	$(2.7 \pm 0.2) \times 10^8$

a) As molar extinction coefficient of $ArA^{\bullet+}$, 14000 $mol^{-1}\,dm^3\,cm^{-1}$ at 1280 nm was employed.[50]

between $P_{Zn}{}^{\bullet+}$ of $3P_{Zn}$ and neutral ArA molecule, the remaining two P_{Zn} moieties do not hinder an approach of ArA molecule, supporting a slight delocalization of the hole of $P_{Zn}{}^{\bullet+}$ to the neighboring P_{Zn} moieties.

After reaching maximal concentration, $ArA^{\bullet+}$ began to decay in long time-scale measurements, indicating that final back electron transfer after hole transfer ($k_{fbet}{}^{ht}$) takes place between $ArA^{\bullet+}$ and $C_{60}{}^{\bullet-}$, returning to ArA, C_{60}, and nP_{Zn}. The decay of $ArA^{\bullet+}$ obeys second-order kinetics; the $k_{fbet}{}^{ht}$ values were evaluated to be $(2.7–2.8) \times 10^8$ $mol^{-1}\,dm^3\,s^{-1}$ for nP_{Zn}, which are one order smaller than the k_{diff} value in PhCN. Even for the oppositely charged species, the final back electron-transfer process after hole transfer is appreciably slowed down compared with the $k_{bet}{}^{2nd}$ values between $nP_{Zn}{}^{\bullet+}$ and $C_{60}{}^{\bullet-}$, because of the lower oxidation potential of ArA. Since no dendrimer effect was observed for the $k_{fbet}{}^{ht}$ values, back electron transfer between $ArA^{\bullet+}$ and $C_{60}{}^{\bullet-}$ takes place outside of the effect of nP_{Zn}.

Summary

In the present study, we demonstrate effects of the dendrimer generation on the photoinduced intermolecular processes of nP_{Zn} (n = 1, 3, and 7). In the intramolecular processes, the lifetimes of the $^3nP_{Zn}{}^*$ states are not significantly changed with the dendrimer generation. The intermolecular T–T annihilation process was slowed down with the dendrimer generation, which was well interpreted by the localization of the $^3P_{Zn}{}^*$ state almost on a unit in nP_{Zn}. In the electron-transfer

processes from the excited triplet states of nP_{Zn} to C_{60} in PhCN, the k_{et}^{obs} value for $^37P_{Zn}$* is larger than those of $^31P_{Zn}$* and $^33P_{Zn}$*. This result is attributed to the increase of the effective radius due to a slight delocalization of the $^3P_{Zn}$* state and to the C_{60}-trapping ability of $^37P_{Zn}$*. In the back electron-transfer process between the oppositely charged species, a small dendrimer generation effect was observed. In the hole-transfer process occurring between the charge species and neutral molecules, a smooth increase of the k_{hs} values with the dendrimer generation was observed, suggesting the delocalization of the hole to the neighboring P_{Zn} moieties.

The authors are grateful to a financial support by a Grant-in-Aid of Scientific Research on Priority Areas (417) from the Ministry of Education, Culture, Sports, Science and Technology and by the Mitsubishi Foundation.

References

1 R.-H. Jin, T. Aida, and S. Inoue, *J. Chem. Soc., Chem. Common.*, **1993**, 1260.

2 J. S. Lindsey, S. Prathapan, T. E. Johnson, and R. W. Wangner, *Tetrahedron*, **50**, 8941 (1994).

3 R. W. Wagner, T. E. Johnson, F. Li, and J. S. Lindsey, *J. Org. Chem.*, **60**, 5266 (1995).

4 D. L. Jiang and T. Aida, *Chem. Commun.*, **1996**, 1523.

5 R. Sadamoto, N. Tomioka, and T. Aida, *J. Am. Chem. Soc.*, **118**, 3978 (1996).

6 P. Bhyrappa, J. K. Young, J. S. Moore, and K. S. Suslick, *J. Am. Chem. Soc.*, **118**, 5708 (1996).

7 T. Norsten and N. Branda, *Chem. Commun.*, **1998**, 1257.

8 T. Aida, D. L. Jiang, E. Yashima, and Y. Okamoto, *Thin Solid Films*, **331**, 254 (1998).

9 K. W. Pollak, J. W. Leon, J. M. J. Frechet, M. Maskus, and H. D. Abruna, *Chem. Mater.*, **10**, 30 (1998).

10 K. W. Pollak, E. M. Sanford, and J. M. J. Frechet, *J. Mater. Chem.*, **8**, 519 (1998).

11 O. Mongin, C. Papamicae, N. Hoyler, and A. Gossauer, *J. Org. Chem.*, **63**, 5568 (1998).

12 C. C. Mak, D. Pomeranc, M. Montalti, L. Prodi, and J. K. M. Sanders, *Chem. Commun.*, **1999**, 1083.

13 T. Kato, M. Uchiyama, N. Maruo, T. Arai, and N. Nishino, *Chem. Lett.*, **2000**, 144.

14 M. S. Matos, J. Hofkens, W. Verheijen, F. C. De Schryver, S. Hecht, K. W. Pollak, J. M. J. Frechet, B. Forier, and W. Dehaen, *Macromolecules*, **33**, 2967 (2000).

15 B. P. Singh, R. Vijaya, S. J. Shetty, K. Kandasamy, P. N. Puntambekar, and T. S. Srivastava, *J. Porphyrins Phthalocyanines*, **4**, 659 (2000).

16 P. Weyermann and F. Diederich, *J. Chem. Soc., Perkin Trans. 1*, **2000**, 4231.

17 J. F. Eckert, D. Byrne, J. F. Nicoud, L. Oswald, J. F. Nierengarten, M. Numata, A. Ikeda, S. Shinkai, and N. Armaroli, *New J. Chem.*, **24**, 749 (2000).

18 M. S. Choi, T. Aida, T. Yamazaki, and I. Yamazaki, *Angew. Chem., Int. Ed.*, **40**, 3194 (2001).

19 C. S. Rajesh, G. J. Capitosti, S. J. Cramer, and D. A. Modarelli, *J. Phys. Chem. B*, **105**, 10175 (2001).

20 S. Van Doorslaer, A. Zingg, A. Schweiger, and F. Diederich, *ChemPhysChem*, **3**, 659 (2002).

21 V. Rozhkov, D. Wilson, and S. Vinogradov, *Macromolecules*, **35**, 1991 (2002).

22 G. J. Capitosti, C. D. Guerrero, D. E. Binkley, C. S. Rajesh, and D. A. Modarelli, *J. Org. Chem.*, **68**, 247 (2003).

23 O. Finikova, A. Galkin, V. Rozhkov, M. Cordero, C. Hagerhall, and S. Vinogradov, *J. Am. Chem. Soc.*, **125**, 4882 (2003).

24 R. Ballardini, B. Colonna, M. T. Gandolfi, S. A. Kalovidouris, L. Orzel, F. M. Raymo, and J. F. Stoddart, *Eur. J. Org. Chem.*, **2003**, 288.

25 N. Armaroli, *Photochem. Photobiol. Sci.*, **2**, 73 (2003).

26 J.-F. Nierengarten, "Fullerenes: From Synthesis to Optoelectronic Properties," ed by D. M. Guldi and N. Martín, Kluwer, The Netherland (2002), Vol. 4, pp. 51–79.

27 T. Nojiri, A. Watanabe, and O. Ito, *J. Phys. Chem. A*, **102**, 5215 (1998).

28 M. E. El-Khouly, S. D.-M. Islam, M. Fujitsuka, and O. Ito, *J. Porphyrins Phthalocyanines*, **4**, 713 (2000).

29 M. E. El-Khouly, Y. Araki, M. Fujitsuka, and O. Ito, *Photochem. Photobiol.*, **74**, 22 (2001).

30 M. E. El-Khouly, Y. Araki, M. Fujitsuka, and O. Ito, *Phys. Chem. Chem. Phys.*, **4**, 3322 (2002).

31 M. Kimura, T. Shiba, M. Yamazaki, K. Hanabusa, H. Shirai, and N. Kobayashi, *J. Am. Chem. Soc.*, **123**, 5636 (2001).

32 X. Camps, E. Dietel, A. Hirsch, S. Pyo, L. Echegoyen, S. Hackbarth, and B. Röder, *Chem.—Eur. J.*, **5**, 2362 (1999).

33 D. Kuciauskas, P. A. Liddell, S. Lin, T. E. Johnson, S. J. Weghorn, J. S. Lindsey, A. L. Moore, T. A. Moore, and D. Gust, *J. Am. Chem. Soc.*, **121**, 8604 (1999).

34 G. Kodis, P. A. Liddell, L. de la Garza, P. C. Clausen, J. S. Lindsey, A. L. Moore, T. A. Moore, and D. Gust, *J. Phys. Chem. A*, **106**, 2036 (2002).

35 M. S. Choi, T. Aida, H. Luo, Y. Araki, and O. Ito, *Angew. Chem., Int. Ed.*, **42**, 4060 (2003).

36 L. Pekkarimen and H. Linschitz, *J. Am. Chem. Soc.*, **82**, 2407 (1960).

37 I. Carmichael and G. L. Hug, *J. Phys. Chem. Ref. Data*, **15**, 1 (1986).

38 K. Kikuchi, "Triplet–Triplet Absorption Spectra," Bunshin Publishing, Tokyo (1989).

39 G. A. Heath, J. E. McGrady, and R. L. Martin, *J. Chem. Soc., Chem. Commun.*, **1992**, 1272.

40 E. F. Zwicker and L. I. Grossweiner, *J. Phys. Chem.*, **67**, 549 (1963).

41 S. L. Murov, I. Carmichael, and G. L. Hug, "Handbook of Photochemistry," 2nd ed, Marcel Dekker, New York (1993), p. 208.

42 P. W. Atokins, "Physical Chemistry," 4th ed, Oxford University Press (1990).

43 S. A. Nonell. J. W. Arbogast, and C. S. Foote, *J. Phys. Chem. A*, **102**, 5215 (1998).

44 J. W. Arbogast, C. S. Foote, and M. Kao, *J. Am. Chem. Soc.*, **114**, 2277 (1992).

45 D. Rehm and A. Weller, *Isr. J. Chem.*, **8**, 259 (1970).

46 Although intramolecular electron transfer process may increase with the increases in the concentrations, quenching of $^3nP_{Zn}$* by C_{60} is predominant under our experimental conditions such as nP_{Zn} less than 0.05 mmol dm^{-3} and C_{60} less than 0.15 mmol dm^{-3} which is a limit of solubility in PhCN.

47 C. A. Steren, H. von Willigen, L. Biczok, N. Gupta, and H. Linschitz, *J. Phys. Chem.*, **100**, 8920 (1996).

48 M. M. Alam, O. Ito, N. Sakurai, and H. Moriyama, *Res. Chem. Intermed.*, **25**, 323 (1999).

49 S. Fukuzumi, K. Ohkubo, H. Imahori, and D. M. Guldi, *Chem.—Eur. J.*, **9**, 1585 (2003).

50 Y. Sasaki, O. Ito, Y. Araki, M. Fujitsuka, A. Hirao, and H. Nishizawa, *Photochem. Photobiol. Sci.*, **2**, 136 (2003).